Thermal Stability and DPPC/Ca^{2+} Interactions of Pulmonary Surfactant SP-A from Bulk-Phase and Monolayer IR Spectroscopy†

Xiaohong Bi,‡ Svetla Taneva,§ Kevin M. W. Keough,§ Richard Mendelsohn,*,‡ and Carol R. Flach*,‡

Department of Chemistry, Newark College of Arts and Science, Rutgers University, 73 Warren Street, Newark, New Jersey 07102, and Departments of Biochemistry and Discipline of Pediatrics, Memorial University of Newfoundland, St. John's Newfoundland A1B 3X9, Canada

Received June 8, 2001; Revised Manuscript Received September 10, 2001

ABSTRACT: Surfactant protein A (SP-A), the most abundant pulmonary surfactant protein, is implicated in multiple biological functions including surfactant homeostasis, biophysical activity, and host defense. SP-A forms ternary complexes with lipids and Ca^{2+} which are important for protein function. The current study uses infrared (IR) transmission spectroscopy to investigate the bulk-phase interaction between SP-A, 1,2-dipalmitoylphosphatidylcholine (DPPC), and Ca^{2+} ions along with IR reflection−absorption spectroscopy (IRRAS) to examine protein secondary structure and lipid orientational order in monolayer films in situ at the air/water interface. The amide I contour of SP-A reveals two features at 1653 and 1636 cm^{-1} arising from the collagen-like domain and a broad feature at 1645 cm^{-1} suggested to arise from the carbohydrate recognition domain (CRD). SP-A secondary structure is unchanged in lipid monolayers. Thermal denaturation of SP-A in the presence of *either* DPPC *or* Ca^{2+} ion reveals a sequence of events involving the initial melting of the collagen-like region, followed by formation of intermolecular extended forms. Interestingly, these spectral changes were inhibited in the ternary system, showing that the combined presence of *both* DPPC *and* Ca^{2+} confers a remarkable thermal stability upon SP-A. The ternary interaction was revealed by the enhanced intensity of the asymmetric carboxylate stretching vibration. The IRRAS measurements indicated that incorporation of SP-A into preformed DPPC monolayers at a surface pressure of 10 mN/m induced a decrease in the average acyl chain tilt angle from 35° to 28°. In contrast, little change in chain tilt was observed at surface pressures of 25 or 40 mN/m. These results are consistent with and extend the fluorescence microscopy studies of Keough and co-workers [Ruano, M. L. F., et al. (1998) *Biophys. J. 74*, 1101−1109] in which SP-A was suggested to accumulate at the liquid-expanded/liquid-condensed boundary. Overall these experiments reveal the remarkable stability of SP-A in diverse, biologically relevant environments.

Pulmonary surfactant, a lipid−protein complex, constitutes the thin layer lining the epithelium of the lung. The unique composition of surfactant serves to stabilize this biological interface, facilitate respiration, and contribute to the host defense system of the lung (*1*). The composition and function of pulmonary surfactant have been reviewed recently (*2*−*5*). The constituents of surfactant, approximately 90% lipid and 10% protein, are transformed into specific structures as they proceed from the type II cells, where they are produced, to the air/alveolar interface. The predominant phospholipid component, 1,2-dipalmitoylphosphatidylcholine (DPPC),[1] is generally accepted as being responsible for surface tension lowering at the air/alveolar interface which prevents collapse during expiration. Four surfactant proteins (SP) have been isolated. SP-B and SP-C are small, hydrophobic proteins known to facilitate adsorption and spreading at the air/water interface. SP-A and SP-D are multimeric, water-soluble, Ca^{2+}-dependent collectins (collagenous lectins). Multiple functions involving surfactant homeostasis, biophysical activity, and host defense have been attributed to SP-A, the most abundant surfactant protein. This broad range of putative functions is most likely related to the diversity of ligands for SP-A (*6*, *7*).

Native SP-A exists as an oligomeric glycoprotein. Its monomeric structure, with a molecular mass of 26−38 kDa and an isoelectric point of ∼5, is characterized by four distinct domains including a short N-terminal region, a collagen-like domain, a hydrophobic neck region, and a globular carbohydrate recognition domain (CRD). Assembly into a functional octadecamer is thought to proceed via trimerization which involves the formation of both triple

† This work was supported by USPHS Grant GM 29864 (R.M.).

* To whom correspondence should be addressed. Phone: (973) 353-5613. Fax: (973) 353-1264. E-mail: flach@andromeda.rutgers.edu or mendelso@andromeda.rutgers.edu.

‡ Newark College of Arts and Science, Rutgers University

§ Memorial University of Newfoundland.

[1] Abbreviations: IRRAS, infrared reflection−absorption spectroscopy; SP, surfactant protein; DPPC, 1,2-dipalmitoylphosphatidylcholine; DPPC-d_{62}, acyl chain perdeuterated DPPC; CRD, carbohydrate recognition domain; TM, tubular myelin; LC, liquid-condensed; LE, liquid-expanded; π−*A*, surface pressure−molecular area; π_i, initial surface pressure; $\nu_s(CH_2)$, symmetric methylene stretching mode; $\nu_a(CH_2)$, asymmetric methylene stretching mode; $\nu_a(COO^-)$, asymmetric carboxylate stretching mode; TEM, transmission electron microscopy; GIXD, grazing incidence X-ray diffraction; PM, polarization modulation.

10.1021/bi011188h CCC: $20.00
Published on Web 10/18/2001

helices among collagen-like domains and α-helical coiled coils in the neck region (*8, 9*). Trimers associate through several weak noncovalent interactions to form the higher order oligomers and are stabilized by N-terminal interchain disulfide bonds (*8*−*11*). Physiological Ca^{2+} or salt concentrations have been shown to induce self-association or aggregation of SP-A octadecamers (*12, 13*). Aggregation can also be induced by pH values less than 6.0 (*14*).

Of the many biological functions proposed for SP-A, several involve the protein's ability to bind phospholipids and aggregate vesicles in a Ca^{2+}-dependent manner (*6, 15*). Studies have begun to address structure−function relationships for SP-A with regard to lipid interaction. Mutagenesis studies have suggested that the major lipid binding site resides in the C-terminal CRD, also known to contain Ca^{2+} binding sites (*6*). Recent transmission electron microscopy (TEM) investigations of SP-A in association with lipid monolayers are consistent with a Ca^{2+}-dependent interaction between CRDs and the lipid polar headgroups (*16, 17*). Earlier reports, however, proposed a hydrophobic interaction between the neck region of SP-A and the lipid acyl chains (*15, 18*−*20*). It is possible that more than one domain within an SP-A octadecamer interacts with lipids.

SP-A has a preference for gel-state lipids and specifically interacts with DPPC (*15, 20, 21*). This association may play a role in the production of tubular myelin (TM), a lattice-like bilayer complex located in the alveolar hypophase that is widely considered to be the source of the surface-active film in vivo. The production of synthetic forms of TM requires the presence of SP-A, DPPC, and SP-B (*22*). This synergistic relationship between SP-A and SP-B also promotes lipid adsorption to the air/water interface where SP-A has again shown a preference for the more ordered, liquid-condensed (LC) phase of DPPC (*14, 23*−*25*).

The current study was undertaken to investigate the conformation and stability of SP-A in bulk-phase and monolayer environments. Bulk-phase thermal denaturation studies utilizing Fourier transform infrared (FTIR) spectroscopy probe the Ca^{2+}-dependent conformational behavior of the protein in aqueous solutions and in lipid dispersions. IR spectroscopy also provides a convenient means to detect changes in lipid-phase state both in bulk phases and in monolayers. In addition, recent developments in infrared reflection−absorption spectroscopy (IRRAS) permit an evaluation of protein secondary structure upon adsorption to the surface and the determination of lipid acyl chain orientation (average tilt angle of the acyl chains with respect to the surface normal) in situ at the air/water interface (*26*−*29*). Orientational parameters are derived from the dependence of the reflected intensities of plane-polarized light on the angle of incidence (angle between the incident beam and surface normal) (*30*).

MATERIALS AND METHODS

Materials. DPPC and acyl chain perdeuterated DPPC (DPPC-d_{62}) were purchased from Avanti Polar Lipids (Alabaster, AL). Chloroform, methanol, EDTA, and HPLC-grade water were obtained from Fisher Scientific (Pittsburgh, PA). Trizma [tris(hydroxymethyl)aminomethane] hydrochloride, $CaCl_2 \cdot 2H_2O$, and sodium chloride were purchased from Sigma (St. Louis, MO). D_2O with 99.9% isotopic enrichment was purchased from Cambridge Isotope Laboratories (Andover, MA).

Protein Isolation and Purification. Porcine SP-A was prepared as previously described (*31*). Briefly, pig lungs were lavaged with 0.15 M NaCl, and the lavage was centrifuged at 800*g* for 10 min. The supernatant was centrifuged at 7000*g* for 60 min. SP-A was purified from the surfactant pellet by extraction with 1-butanol (*31, 32*). SDS−polyacrylamide gel electrophoresis (12% gel) was performed on samples of SP-A solutions according to the method of Laemmli (*33*) followed by staining with Coomassie Blue. Under reducing conditions (5% β-mercaptoethanol), a major band at ∼36 kDa and a minor band at ∼28 kDa were observed. Variable glycosylation in the C-terminal region of SP-A produces the observed polymorphic molecular mass (*32*).

Bulk-Phase FTIR Sample Preparation and Spectroscopy. Porcine SP-A was dissolved in 5 mM HEPES buffer, pH 6.9, at a concentration of ∼0.8 mg/mL. Two hundred microliters of the SP-A stock solution was concentrated to about 30 μL in an Amicon Microcon-10 microconcentrator (Beverly, MA) by spinning in an Eppendorf model 5415C microcentrifuge (Eppendorf-Netheler-Hinz GmbH, Westbury, NY) at 14 000 rpm. The concentrated solution was diluted by adding 400 μL of D_2O buffer (5 mM Tris, 0.1 mM EDTA, pD 6.9). After three cycles of dilution and spinning to 30 μL, the SP-A sample (in D_2O buffer) was collected at a final concentration of ∼5 mg/mL, sufficient for IR bulk-phase measurements. For experiments performed in the presence of Ca^{2+}, 1 μL of a $CaCl_2$ stock solution in D_2O was added to achieve a final concentration of 1.5 mM Ca^{2+}, close to the concentration of Ca^{2+} in the hypophase environment lining the lung (*34*). Multilamellar lipid vesicles were prepared by rehydration of a nitrogen-dried DPPC-d_{62} lipid film with the concentrated SP-A solution, yielding a 25/1 lipid/SP-A molar ratio.

Samples for FTIR were placed between AgCl windows separated with a 25 μm spacer. A thermostated transmission cell (Harrick Scientific, Ossining, NY) was used with a circulating water bath, and temperatures were monitored with a digital thermocouple (Physitemp Instruments, Clifton, NJ) accurate to ±0.1 °C. Bulk-phase FTIR spectra were collected on a Mattson Instruments Research Series (RS-1) spectrometer equipped with an MCT detector and a sample shuttle. The spectrometer was under constant dry air purge. Eight blocks of 128 scans of sample and air background were co-added into separate files to produce IR spectra with optimal water compensation. Spectra were acquired at 4 cm^{-1} resolution, apodized with a triangular function, and Fourier-transformed with one level of zero-filling to yield data encoded every 2 cm^{-1}. Spectra of D_2O buffer were acquired at the appropriate temperatures to use for background subtraction.

Monolayer Preparation and IRRAS Measurements. A custom-designed Langmuir trough (Nima Technology, Inc., Coventry, England) with a Nima model PS4 surface pressure sensor was used for the monolayer experiments. The features of the trough shown in Figure 1A have been described in detail elsewhere (*27*). The trough has been designed to permit subphase injection of aqueous solutions without disturbing a preexisting monolayer and to inhibit the diffusion of solutes to the background side of the trough. The trough has two independently controlled barriers and a center divider, the

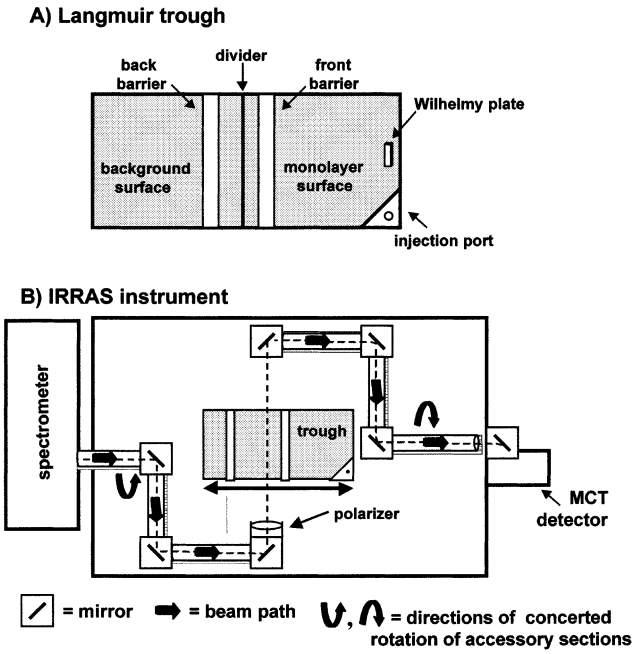

FIGURE 1: (A) Design of the Langmuir trough used in the current studies. The trough is shuttled under computer control for IR illumination of the background surface and monolayer covered surface. (B) Schematic of the IRRAS instrument displaying the sections of the accessory that rotate in concert under computer control to provide the desired angle of incidence.

top of which lies just beneath the water surface. Injections are made when the back barrier is positioned over the divider which leaves a small gap of ~0.25 mm. This retards the rate of solute diffusion to the background side while maintaining an equal subphase height on either side of the barrier for acquisition of high-quality IRRAS spectra.

The subphase consisted of 150 mM NaCl, 5 mM Tris, and either 0.1 mM EDTA or 1.5 mM $CaCl_2$, pH (or pD) 6.9, in HPLC water (or D_2O). The temperature of the subphase was held at 21.5 ± 0.5 °C. Conducting IRRAS experiments at 37 °C is not feasible because of enhanced interference from the rotational−vibrational modes of H_2O or HDO vapor in spectral regions of interest, compared to 21.5 °C. In addition, evaporation of the subphase at 37 °C would affect the subphase height during the course of the experiment, altering the optical alignment. DPPC monolayers were formed by the dropwise spreading of 5−10 μL of a 1 mg/mL lipid/chloroform solution onto a clean surface at the maximum surface area (86.0 cm^2) for the trough. At least 30 min was allowed for solvent evaporation and film relaxation/equilibration. The initial surface pressure (prior to compression) for all experiments was 0 mN/m. Films were continuously compressed at a speed of ~0.02 nm^2/(molecule·min) while surface pressure−molecular area (π−A) isotherms were recorded. When the desired surface pressure was reached, the films were again allowed to relax for at least 30 min prior to IR data collection from the pure lipid monolayer. For studies of SP-A adsorption, 75 μL of aqueous protein solution (~0.8 mg/mL) was injected beneath the preformed monolayer of DPPC with the back barrier positioned over the divider. When the surface pressure had stabilized (~30 min), IRRAS spectra of the lipid/protein film were acquired. Within the IRRAS spectra acquisition time, there was no indication of protein diffusion to the reference side of the trough. In one set of experiments, conducted on the EDTA/D_2O-buffered subphase, a subsequent injection of a concentrated $CaCl_2$ solution was made (1.5 mM final Ca^{2+} concentration in subphase), and additional IRRAS spectra of the DPPC/SP-A film were obtained.

IRRAS spectra were acquired with a Bruker Instruments Equinox 55 Spectrometer equipped with an external variable angle reflectance accessory, the XA51. A schematic of the IRRAS instrument is shown in Figure 1B. The accessory is a self-contained computer-controlled unit attached to the external port on the spectrometer (*27*). The instrument allows for the acquisition of spectra over a range of incident angles which are obtained by rotating the arms of the accessory above the trough as shown in Figure 1B. S- or p-polarized radiation is generated using a wire grid polarizer that is inserted in the beam path just before the water surface. The system is aligned so that the IR beam is focused onto the water surface, and the reflected light is then collected and directed onto a narrow-band mercury cadmium telluride (MCT) detector. The entire experimental setup is enclosed and purged to keep the relative humidity levels both low and as constant as feasible.

A computer-controlled sample shuttle allows interferograms from the background side (aqueous surface) and from the sample side (monolayer surface) to be collected in alternating fashion. The number and size of co-added interferogram blocks can be varied to provide a high signal-to-noise ratio and to compensate for water vapor. A time delay of 20 s was allowed for film equilibration between trough movement and data collection. Typically, 1 block of 512 scans was collected for the films at all angles of incidence when the lipid CH_2 stretching modes were being quantitatively monitored while a single block of 1024 scans provided excellent water vapor compensation for the amide I region of SP-A adsorbed films. Interferograms were collected at either 4 or 8 cm^{-1} resolution, co-added, apodized with a Blackman-Harris-3-term function, and fast Fourier-transformed with one level of zero-filling. Spectra were acquired over a range of incident angles using p-polarized radiation followed by data collection using s-polarized light. IRRAS spectra are reported as $-\log (R/R_o)$ where R is the intensity of light reflected from the film-covered surface and R_o is the intensity of light reflected from the background surface.

Bulk-Phase FTIR and IRRAS Data Analysis. Spectral subtraction and baseline leveling were carried out as needed using Grams/32 (Galactic Industries Corp., Ithaca, NY). Fourier deconvolution was performed and peak positions were determined using a center of gravity algorithm provided by the National Research Council of Canada (*35*). Two-dimensional (2D)-IR analysis was performed on the bulk-phase IR spectra in the amide I region to enhance the resolution of overlapped components. A 2D-IR spectrum is generated by applying correlation analysis to the dynamic fluctuations in IR intensities caused by an external perturbation. In the current case, the perturbation is temperature. Prior to analysis, a matching buffer spectrum was subtracted from each sample spectrum, and the resultant spectra were truncated to include the region of interest (1580−1700 cm^{-1}). The spectra were also normalized within this spectral region to compensate for sample density changes with increasing temperature. A home-written version of the 2D algorithm

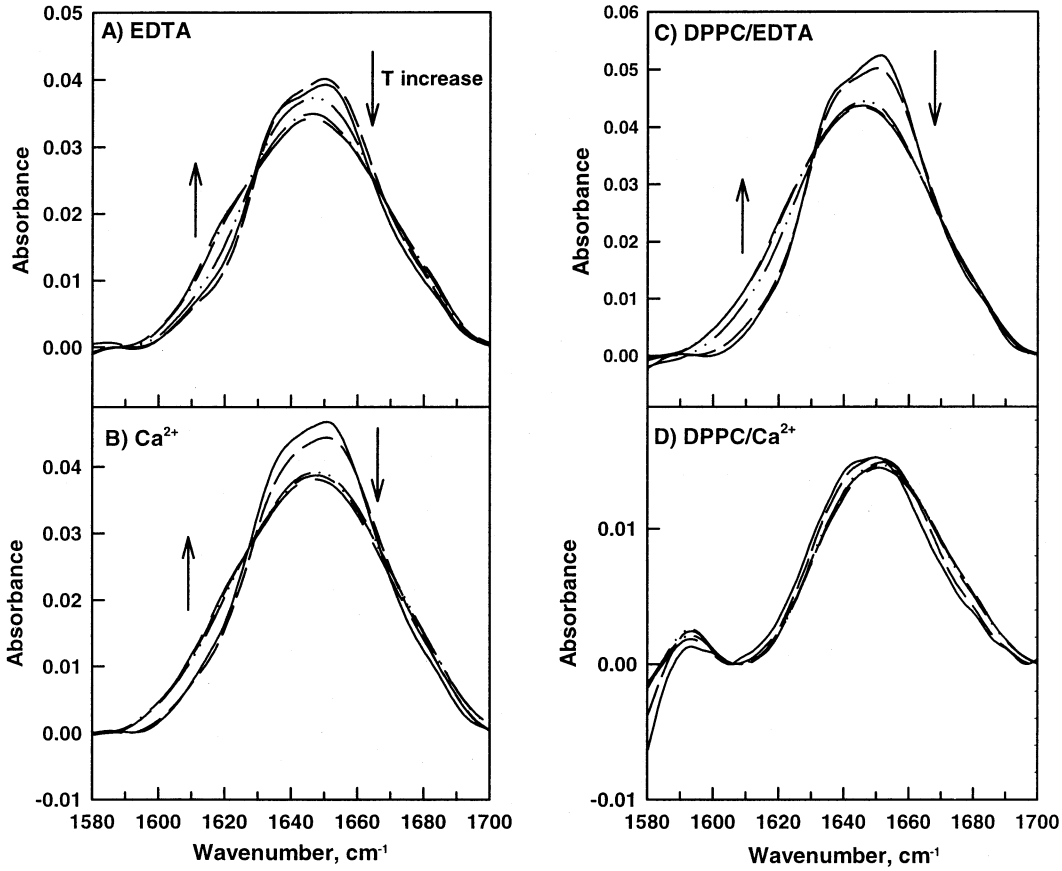

FIGURE 2: IR spectra of the 1580−1700 cm^{-1} region for SP-A in EDTA buffer (A), Ca^{2+} buffer (B), with DPPC in EDTA buffer (C), and with DPPC in Ca^{2+} buffer (D), at a series of temperatures as follows in each instance: 25 °C (—), 50 °C (- - -), 65 °C (— ·· —), 70 °C (— · —), and 75 °C (— —). The direction of the arrows shows the spectral changes as temperatures are increased.

described by Noda (*36*) was used where the spectra are combined in an intensity matrix that is subsequently Fourier-transformed. The intensity variations at each wavenumber position are then plotted in a pairwise fashion (*37*).

IRRAS Simulations. Quantitative evaluation of the symmetric methylene stretching band [$\nu_s(CH_2)$] intensities obtained at various incident angles using s- and p-polarized radiation is used to determine the average lipid acyl chain tilt angle. The methods have been previously described (*26, 27, 30*). In brief, the mathematical formalism of Kuzmin and Michailov (*38, 39*) was applied which requires knowledge of the optical constants for the subphase and the monolayer including both the real and the imaginary parts of the refractive index. Values for H_2O are obtained from Bertie et al., 1989 (*40*). The real part of the refractive index for the monolayer has been obtained from IR ellipsometric measurements of thin films on solid supports (A. Roseler, unpublished results) and is assumed to be isotropic. The imaginary part of the refractive index for the monolayer (scale factor) is related to the extinction coefficient for the vibrational mode and the density of the film-forming molecules on the surface. The directional components of this value are calculated using Fraser's model for uniaxial symmetry (*41*). Fraser's model also requires the angle between the transition dipole moment change and the molecular axis [90° for the $\nu_s(CH_2)$ mode with respect to an all-trans acyl chain] and the acyl chain tilt angle as input parameters. We have found that the polarizer efficiency must also be taken into consideration and have previously determined this value to be ~0.8% in the wavenumber range of interest (*27*). The simulation is run in an iterative fashion until a combination of scale factor and tilt angle fits the experimental data for s- and p-polarized radiation over a range of incident angles less than the Brewster angle.

RESULTS

Bulk-Phase FTIR. Spectra of the amide I region for SP-A in Tris buffer containing 0.1 mM EDTA or 1.5 mM calcium chloride at several temperatures are shown in Figure 2A,B, respectively. The corresponding spectra in the presence of DPPC-d_{62} multilamellar vesicles are shown in Figure 2C,D. The broad amide I band, arising primarily from the peptide bond C═O stretching mode, is centered at ~1648 cm^{-1} and clearly contains several underlying components due to various secondary structures in the protein. The current assignment of amide I frequencies to particular secondary structures is based upon the putative structure of SP-A, well-established IR amide I band correlations (*42*), and CD measurements for SP-A (*8, 11*). In addition, Fourier deconvolution and 2D-IR (*36, 37*) are used to enhance the resolution of the constituent bands in the original spectra. 2D-IR also provides information about the response of spectral intensity variations to perturbation, e.g., temperature, in the current instance.

Similar temperature-induced changes are observed in the amide I region both for pure protein samples and for the DPPC/SP-A vesicles in the absence of calcium ion (Figure 2A−C). Underlying components within the amide I region are evident in the deconvolved spectra for these samples

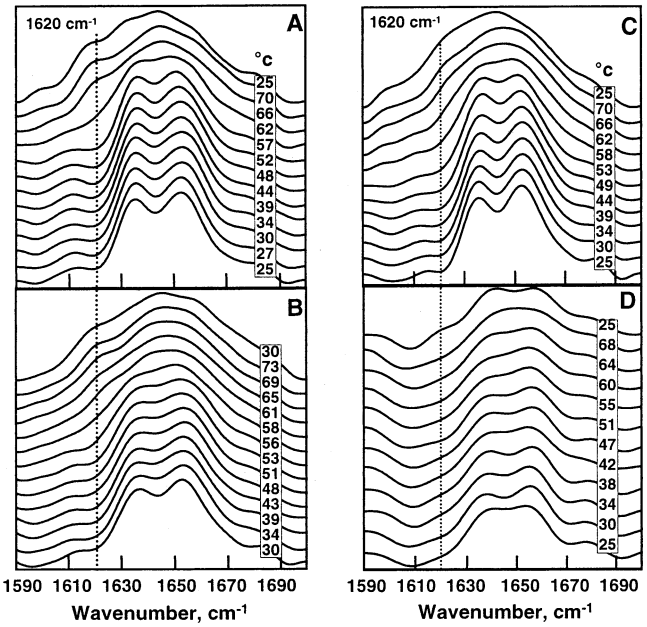

FIGURE 3: Deconvolved spectra of SP-A in EDTA buffer (A), Ca^{2+} buffer (B), with DPPC in EDTA buffer (C), and with DPPC in Ca^{2+} buffer (D) with temperature (°C) as shown in the figure. The top spectrum in each plot was acquired after the sample was cooled to either 25 or 30 °C. The deconvolution parameters were full-width at half-height = 19 cm^{-1} and $k = 1.8$.

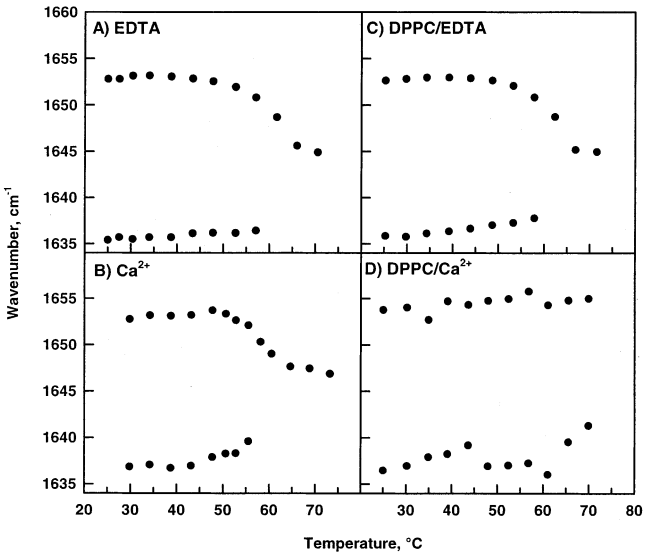

FIGURE 4: Temperature dependence of the amide I region frequencies for SP-A as obtained from deconvolved spectra in EDTA buffer (A), Ca^{2+} buffer (B), with DPPC in EDTA buffer (C), and with DPPC in Ca^{2+} buffer (D).

shown in Figure 3A−C with the peak positions obtained from the deconvolved spectra plotted as a function of temperature in Figure 4A−C. The frequencies of the two dominant bands observed at ∼1653 and ∼1636 cm^{-1} remain essentially unchanged as the temperature is increased from 25 to 50 °C. At temperatures between 50 and 65 °C, the two bands coalesce into a broad feature centered at ∼1645 cm^{-1}. This process is most likely due to melting of the collagen-like region in SP-A to an unordered/random coil structure. The assignment is supported by both IR measurements of collagen-containing peptides (*43*) and CD measurements of SP-A (*8*, *11*). With further increases in temperature (>60 °C), a shoulder at ∼1620 cm^{-1} develops, presumably due

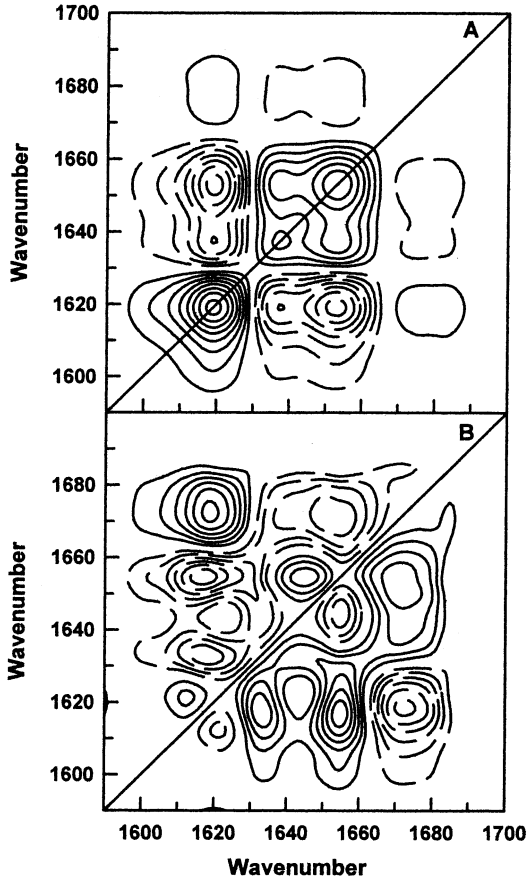

FIGURE 5: Synchronous (A) and asynchronous (B) 2D-IR plots for SP-A in EDTA buffer. Solid and dashed lines represent positive and negative bands, respectively. The 2D-IR analysis was performed over a series of spectra acquired as a function of temperature.

to intermolecular β-sheet structure or aggregation of the protein. The temperature-dependent changes in the amide I region are irreversible as seen in the deconvolved spectra obtained after recooling (Figure 3A−C, top trace).

2D-IR analysis was also performed on the amide I region for these three samples to enhance the spectral resolution and determine whether changes in the constituent amide I components respond to the temperature increase in a correlated or uncorrelated manner. 2D-IR plots, synchronous (correlated) and asynchronous (uncorrelated), are shown for the SP-A/EDTA sample in Figure 5A,B, respectively. Application of the 2D-IR algorithm to the set of IR spectra for SP-A/Ca^{2+} and DPPC/SP-A/EDTA preparations (not shown) displayed similar results to those in Figure 5. In the figure, the solid and dashed contour lines indicate positive and negative changes in the cross-peaks, respectively. The frequencies of paired constituent bands are read off the two orthogonal axes. Auto-peaks found along the diagonal in the synchronous plot are always positive. Their magnitude measures the extent of the spectral intensity variation between the minimum and maximum temperatures used. Cross-peaks located off the diagonal in both plots represent synchronous or asynchronous correlation pairs. For example, the negative, synchronous correlation pair observed at 1653/1620 cm^{-1} (Figure 5A) indicates that the intensity variations in these two components are correlated and occur in opposite directions as the temperature is increased. The cross-peaks in the asynchronous plot reveal additional information about the sequential nature of the intensity variations. Noda has

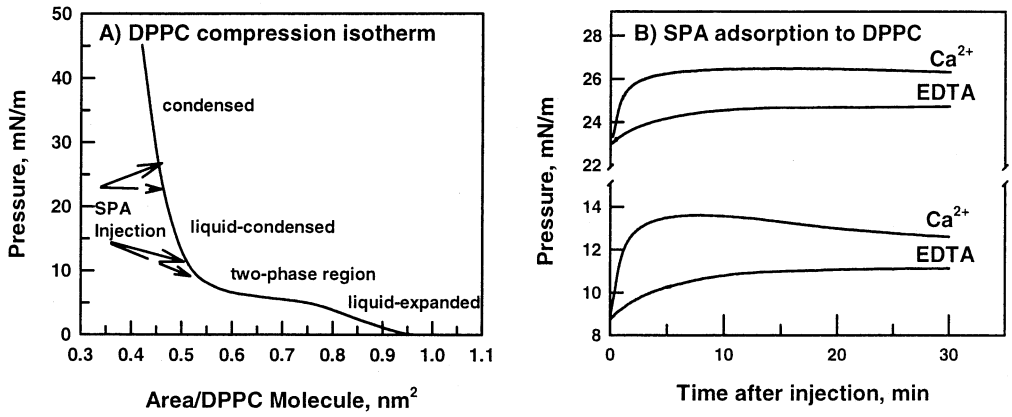

FIGURE 6: (A) Surface pressure−molecular area (π−A) compression isotherm of DPPC at the air−water interface. The double arrows indicate the surface pressure values at which the barrier was stopped (solid) and after a 30 min equilibration period (dashed) for two separate experiments. (B) Adsorption isotherms following injection of SP-A beneath preformed DPPC monolayers at surface pressure values of ~9 and 23 mN/m in EDTA and in Ca^{2+}-containing buffers.

developed a set of rules to determine the temporal sequence of intensity variations disclosed by asynchronous cross-peaks (*36*).

While both plots confirm the correlated and sequential transitions in the amide I region as described above, additional information about the peak at ~1645 cm^{-1} is gained from the 2D-IR analysis. The asynchronous plot indicates that the sequential relationship between the components within each of the following pairs cannot be determined: 1645/1620 cm^{-1} and 1645/1653 cm^{-1}. This, along with the absence of an autopeak at ~1645 cm^{-1} in the synchronous plot, reveals that the 1645 cm^{-1} component is present at all temperatures and that its intensity does not change significantly over the temperature range studied. It seems reasonable to suggest that the broad 1645 cm^{-1} component arises mostly from the globular carbohydrate recognition domain (containing 40−50% of the amino acids in SP-A) and to a lesser extent from particular vibrational modes of the collagen-like domain both before and after melting.

This rich thermotropic behavior is in marked contrast to the stability observed in the amide I region for the DPPC/SP-A vesicles in the presence of Ca^{2+}. The predominant underlying components in the amide I band for the DPPC/SP-A/Ca^{2+} dispersions are observed at ~1655 and 1638 cm^{-1}, and they do not change as the temperature increases from 25 to 70 °C (Figures 3D and 4D). The emergence of the shoulder at 1620 cm^{-1} observed at high temperatures for the other three samples is also absent, and 2D-IR plots (not shown) demonstrate that there are no significant changes in the amide I band constituent intensities over the temperature range studied. The specific interaction between the three sample components evidently inhibits the thermal denaturation of SP-A. Furthermore, an additional band is observed in the DPPC/SP-A/Ca^{2+} spectra which is not found in the other three samples. This feature located at ~1592 cm^{-1} (Figure 2D) arises from the carboxylate asymmetric stretch of Glu and Asp side chains (*44*, *45*) and reveals one aspect of the molecular nature of the stabilizing interaction. Although the acidic amino acid side chains for all samples are expected to be unprotonated at the pD of the buffer used, the intensity of this mode is enhanced only in the DPPC/SP-A/Ca^{2+} sample, indicating that a different carboxylate−counterion interaction takes place in this particular sample. Glu195, Glu202, and Asp215 in the carbohydrate recognition domain of SP-A have all been implicated in Ca^{2+}-dependent lipid binding and aggregation (*46*).

The lipid-phase transition (gel to liquid-crystalline) temperature was found to be independent of the presence of calcium ion, consistent with previous reports. In the presence of SP-A, the melt was initiated at the same temperature; however, the cooperativity of the transition decreased both in the EDTA- and in the Ca^{2+}-containing samples (not shown).

Investigation of SP-A Interaction with DPPC in Monolayers. A typical surface pressure−molecular area (π−A) compression isotherm for a DPPC monolayer acquired using the IRRAS trough is shown in Figure 6A. Two pairs of arrows mark surface pressures where the barrier was stopped and after a 30 min equilibration period in two separate experiments prior to IRRAS data collection and SP-A injection. In both experiments, surface pressure decreased slightly (~2 mN/m) as the lipid monolayer equilibrated, but was constant during the acquisition of IRRAS spectra. Adsorption isotherms obtained after the injection of SP-A into the subphase are shown in Figure 6B. The presence of Ca^{2+} in the subphase induced an increase in the initial rate and magnitude of pressure change upon SP-A adsorption when compared to the EDTA-containing subphase. Adsorption experiments conducted when the DPPC monolayer was at an initial $\pi \approx 10$ mN/m led to a slightly larger increase in pressure compared to those at 25 mN/m. Upon SP-A injection, no further increase in π was observed for a DPPC monolayer compressed to 40 mN/m.

IRRAS spectra of the lipid carbonyl and protein amide I regions acquired using s-polarized radiation at an angle of incidence of 68° for SP-A adsorbed to DPPC monolayers are shown in Figure 7. Two spectra are shown for a DPPC monolayer at an initial pressure (π_i) of ~10 mN/m before and after the injection of Ca^{2+} into the subphase. The additional spectrum displaying the weak amide I band was acquired after SP-A adsorption to DPPC initially at $\pi \approx 25$ mN/m on a Ca^{2+}-free subphase. For the set at $\pi_i \sim 10$ mN/m, a time-dependent increase in the amide I band intensity (~35%) was observed upon the addition of Ca^{2+}, whereas the band position (~1650 cm^{-1}) and full-width at half-height (~40 cm^{-1}) did not change. Surface pressure also increased slightly after injection of Ca^{2+} (~1 mN/m), whereas lipid

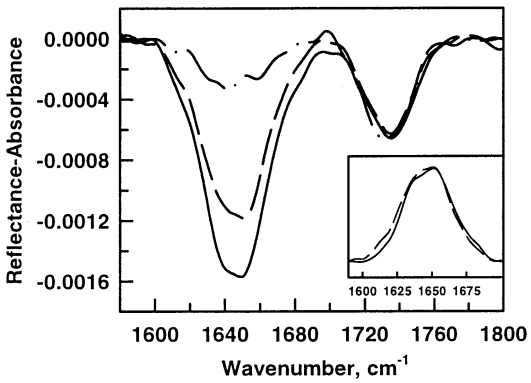

FIGURE 7: IRRAS spectra (s-polarized radiation, 68° angle of incidence) of the 1580−1800 cm^{-1} region for a mixed film after SP-A absorption to a DPPC monolayer at an initial surface pressure (π_i) of 10 mN/m before (− −) and 120 min after (—) injection of Ca^{2+} into the D_2O subphase. The additional overlaid spectrum was acquired after SP-A adsorption to a DPPC monolayer at a π_i of 25 mN/m in EDTA-containing buffer (− · −). The inset shows an inverted and normalized IRRAS spectrum (− −) and a bulk-phase IR spectrum (—) both in the absence of Ca^{2+}.

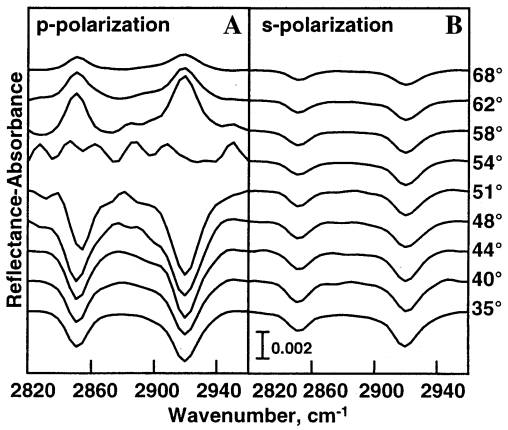

FIGURE 8: IRRAS spectra of the methylene stretching region for a DPPC monolayer acquired at $\pi \sim 10$ mN/m using p- (A) and s-polarized (B) radiation. The angles of incidence are shown at the right of the plot.

carbonyl band shape and position (~1735 cm^{-1}) remained the same both before and after injection of SP-A and Ca^{2+}. The difference in intensity was amplified in separate experiments conducted on either an EDTA- or a Ca^{2+}-containing subphase. For experiments conducted at $\pi_i \sim 10$ mN/m, the presence of Ca^{2+} appears to induce a higher concentration of SP-A in the vicinity of the lipid, near the water surface. This Ca^{2+}-induced increase in amide I band intensity is also observed for DPPC monolayers at $\pi_i \approx 25$ mN/m. However, the intensity of the amide I band relative to the lipid carbonyl for SP-A adsorption to DPPC at $\pi_i \approx 25$ mN/m compared to 10 mN/m is substantially reduced as revealed for the EDTA-containing subphase in Figure 7. The decrease in amide I intensity is also observed for Ca^{2+}-containing subphases when comparing DPPC at $\pi_i \approx 25$ mN/m to 10 mN/m (not shown). The attenuation of both the amide I band intensity and the surface pressure increase upon SP-A adsorption to DPPC at $\pi_i \approx 25$ mN/m compared to 10 mN/m suggests that SP-A is preferentially adsorbed at the lower pressure, where two phases (LE and LC) coexist.

In the inset in Figure 7, the amide I region of the IRRAS spectrum (s-polarized, 68° angle of incidence) on the Ca^{2+}-free buffer has been inverted, normalized, and overlaid with a bulk-phase IR spectrum to illuminate the similarity between the bands in the two extremely different environments. Fourier deconvolution of the amide I band in the spectrum obtained at the air/water interface reveals two components at frequencies 1636 and 1653 cm^{-1}, very similar to the bulk-phase spectra. The structural stability of the lung surfactant protein SP-A at the air/water interface is notable as protein and peptide unfolding or aggregation has often been observed (*47*−*50*). The presence of several secondary structures with overlapping amide I band components in the IRRAS spectra for SP-A precludes a detailed analysis of orientation at the air/water interface. We thus turn to the ordered structure of the acyl chains in DPPC where optical models are well developed for quantitative analysis of chain tilt (*26*, *27*).

Figure 8A,B displays IRRAS spectra of the methylene stretching region for a DPPC monolayer acquired at $\pi \approx 10$ mN/m using s- and p-polarized radiation at several angles of incidence. The symmetric and asymmetric methylene stretching modes [$\nu_s(CH_2)$ and $\nu_a(CH_2)$] are observed at ~2851 and 2920 cm^{-1}, respectively, consistent with a fair degree of chain conformational order. The IRRAS band intensity for the p-polarized data is shown to strongly depend on incident angle. The intensity goes through a minimum at 54°, which is the Brewster angle for the air/water interface in this spectral region. The dependence of the s-polarized data is more subtle; the methylene stretching modes of DPPC are negative at all angles of incidence, and their intensity decreases as the angle of incidence increases. The dependence of the band intensity for the s- and p-polarized spectra on incident angle is used to determine the orientation of the lipid acyl chains (average chain tilt angle with respect to the surface normal).

As previously mentioned, the formalism of Kuzmin and Michailov is applied for the spectral simulations (*38*, *39*). Two parameters, the acyl chain tilt angle and the scale factor, are varied as the simulated reflectance−absorbance values are fit to the experimentally determined $\nu_s(CH_2)$ intensities. The scale factor is treated as a parameter to be analytically determined for a particular vibrational mode and is related to the absorption coefficient and the density of molecules on the surface. The relative magnitude of the molecular density can be obtained from the appropriate $\pi-A$ isotherm. The same scale factor is used for fitting the data before and after injection of SP-A since the number of lipid molecules on the surface does not vary and the frequencies of the $\nu_a(CH_2)$ and $\nu_s(CH_2)$ modes do not change, i.e., the chain conformation is not altered, as the protein is introduced. In addition, the chains are assumed to be conformationally ordered at the surface pressures used here. This assumption is not strictly correct for the lipid acyl chains at a surface pressure of 10 mN/m. This issue will be addressed below.

In Figure 9A,B, the experimentally measured $\nu_s(CH_2)$ mode intensities for DPPC monolayers at different surface pressures on Ca^{2+}-free buffer are compared to those calculated theoretically using s- and p-polarized radiation over a range of incident angles. The simulated intensities that provide the best fit along with the experimental results are shown in Figure 9A for a DPPC monolayer compressed to $\pi = 25$ mN/m before and after the injection of SP-A. The small change observed in the average acyl chain tilt angle (32°→31°) when SP-A adsorbs to the lipid monolayer is

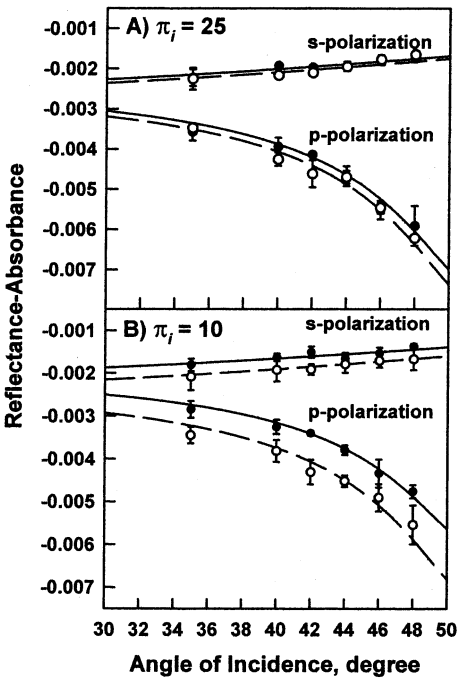

FIGURE 9: Effect of SP-A on the orientation of the DPPC acyl chains measured at surface pressures of 25 mN/m (A) and 10 mN/m (B). The experimentally measured CH_2 symmetric stretching mode intensities for DPPC monolayers on a Ca^{2+}-free buffer are shown before (filled circles) and after SP-A injection (open circles). Solid and dashed lines are the simulated intensities that best fit the experimental results before and after SP-A injection, respectively. The protein induces a significant change in chain tilt only at the lower surface pressure. See text for details.

statistically insignificant (±2°). The best fit to the data at π = 40 mN/m is for an average chain tilt angle of 29 ±1°, independent of the presence of SP-A (not shown). These two chain tilt angles compare well with those derived from grazing incidence X-ray diffraction (GIXD) measurements made at the same pressures (*51*).

The results shown in Figure 9B for a DPPC monolayer compressed to π = 10 mN/m before and after injection of SP-A clearly demonstrate that a change has taken place upon SP-A adsorption, consistent with a decrease in average acyl chain tilt angle. However, since the lipid monolayer at π = 10 mN/m contains a small degree of liquid-expanded phase consisting of acyl chains with gauche rotamers (see isotherm in Figure 6A), the quality of the fit is not as high as for the two experiments conducted at the higher surface pressures. To obtain the best fit to the experimental data at a pressure of 10 mN/m, the range of allowed scale factors has been constrained in a manner consistent with the molecular area change in the π−*A* isotherm. The calculated data used a scale factor that decreased by ~12% compared with that used for the best fit at π = 25 mN/m, where the change in molecular area over this pressure range was ~14% as obtained from the π−*A* isotherm. An average acyl chain tilt angle of 35 ± 3° gave the best fit to the experimental intensities before SP-A injection. After injection, simulations conducted holding the scale factor constant reveal that the chain tilt angle decreased to 28 ± 4°. Other approaches to derive the acyl chain tilt angles, for example, where the scale factor varies freely, also predict a decrease of about the same magnitude in tilt angle upon SP-A adsorption. The relative merits of these methods are currently being evaluated and will be discussed in a subsequent publication. Similar experiments were conducted on a Ca^{2+}-containing subphase where SP-A adsorption again induced a decrease in lipid acyl chain tilt angle, albeit to a slightly lesser extent.

DISCUSSION

Since the efficient function of pulmonary surfactant depends on specific interactions between the surfactant-specific proteins and lipids, a molecular level description of structural changes in these components upon their mutual interaction is of primary importance for understanding surfactant function. Such studies require a reductionist approach with purified components, at least initially. We have selected the major lipid and protein constituents for both bulk-phase and monolayer examination using IR techniques. Thus, the present experiments provide insights into the stability and molecular structures adopted by SP-A and DPPC upon their mutual interaction under physiologically relevant conditions. Although SP-A is known to be intimately associated with DPPC, many gaps remain in the current state of knowledge concerning molecular interactions between the two. The bulk-phase results concerning the structure of SP-A in various environments will first be discussed, followed by comments on the alterations in lipid acyl chain orientation induced by the protein and pressure/Ca^{2+}-dependent differences in SP-A adsorption as observed in the monolayer experiments. Finally, the relevance of these findings to the function of SP-A in vivo will be considered.

Bulk Phase. The Ca^{2+}-induced self-association of SP-A octadecamers and the reversibility of this process after addition of EDTA are well documented from light scattering studies (*12*, *13*, *52*). The level of structural (secondary or tertiary) alteration that accompanies this process is not known with certainty. For example, two previous reports based on Trp fluorescence from residues located in the CRD each suggest that Ca^{2+} binding is accompanied by a conformational change in this region of the protein. However, the results from the two studies differ; Haagsman et al. (*12*) observe an increase in intensity along with a slight shift in the wavelength maximum upon binding whereas Ruano et al. (*52*) report a decrease in intensity without a shift in peak position. In addition, CD measurements of SP-A in the presence and absence of Ca^{2+} show conflicting results. CD spectra of the collagenase-resistant fragment of SP-A containing the Ca^{2+} binding CRD are essentially the same in the presence of EDTA or 2 mM Ca^{2+} (*11*). However, more recent CD investigations reveal Ca^{2+}-induced spectral changes (*52*). Our bulk phase IR results for SP-A suggest that the binding of Ca^{2+} is not accompanied by major secondary structure changes in the protein. This conclusion is based not only on the amide I band characteristics but also on the observation that the thermal denaturation of SP-A proceeds in a similar manner independent of the presence of Ca^{2+}, as revealed by detailed examination of the 2D-IR spectra. The disparities between the results from IR and CD techniques may be due to the increased SP-A concentration required for IR (~5.0 versus ~0.1 mg/mL, respectively) and differing sources of SP-A. This issue is discussed below.

The current bulk-phase IR results also demonstrate that the secondary structure of SP-A in Ca^{2+}-free aqueous

environments remains essentially the same in the presence and absence of DPPC vesicles. This result is consistent with fluorescence measurements which indicated that lipid binding does not alter the hydrophobic environment of the Trp side chains (*15*). However, Casals et al. (*21*) report a decrease in the accessibility of SP-A fluorophores to acrylamide quenching upon interaction with DPPC vesicles. This change in Trp accessibility is again most likely not accompanied by major secondary structure alterations, as revealed by the current detailed 2D-IR analysis of the thermal denaturation of SP-A in the presence and absence of lipid.

It is of interest to attempt to reconcile the differences between the observed IR and CD investigations of SP-A secondary structure alterations induced by Ca^{2+}. IR spectroscopy provides a reasonable means to distinguish between various regular secondary structures. For example, the amide I mode arising from the collagen-like domain in the current work is a doublet at 1653 and 1636 cm^{-1}, while the thermal denaturation of SP-A at high temperature leads to a feature near 1622 cm^{-1}, well-known to arise from extended (e.g., β-sheet) structures. The 2D-IR spectra of SP-A reveal the presence of an additional amide I component near 1645 cm^{-1}, a value appropriate for irregular structures, such as the CRD. This feature is typically very broad. In the current case, this band acted independently from the amide I features arising from the collagen domain. If subtle changes in this spectral region occurred on Ca^{2+} binding, they would tend to be obscured by the more dramatic changes occurring elsewhere in this congested spectral region.

CD spectra are acquired at an order of magnitude lower concentration than IR. Despite this, CD (*11*, *52*) and current IR thermal denaturation studies of SP-A give very similar results. However, discrepancies between the two approaches are noted in the presence of Ca^{2+}. The IR measurements show no changes in secondary structure; the CD data show a large decrease in intensity at 207 nm as Ca^{2+} is added (*52*). Two possibilities seem reasonable. First, it is possible that the CD signals arise in part from the irregular secondary structures in the CRD; these may provide a signal more sensitive to Ca^{2+}-induced changes than the IR amide I mode. Another possibility arises because CD measurements use shorter wavelengths than the IR and require polarized light. The measurements are known to be sensitive to aggregation phenomena, which may affect band positions and intensities. IR measurements are insensitive to intermolecular association of proteins if the secondary structures are unaltered by the association.

The most striking result of the current bulk-phase measurements is the enhanced thermal stability conferred to the protein by the presence of *both* DPPC and Ca^{2+} (i.e., only in the ternary DPPC/SP-A/Ca^{2+} dispersion). The enhanced stability occurs without major changes in the secondary structure of the protein as shown by comparison of the bulk-phase IR spectra of all four samples at room temperature where only minor differences in the conformation-sensitive amide I band profiles are observed (Figures 2 and 3).

The temperature-independent enhanced intensity of the carboxylate asymmetric stretching mode [$\nu_a(COO^-)$] observed only in the ternary complex indicates the involvement of Glu and Asp residues in the stabilizing interaction. Small shifts in the $\nu_a(COO^-)$ peak maximum and intensity changes have been shown to reflect different cation chelation modes (*45*). McCormack and associates have shown that point mutations of particular Glu and Asp residues corresponding to Ca^{2+} coordination sites in the CRD interfere in the association of SP-A with liposomes and with lipid monolayers (*46*, *53*). It was also proposed that SP-A/lipid association occurs between the CRD and phospholipids at the vesicle−solvent interface without substantial penetration of protein into the lipid membrane. It has been suggested that the interaction occurs with CRDs from several individual oligomers (*6*). This mode of interaction is also consistent with our observation that the temperature-induced lipid-phase transition is only slightly altered in the presence of protein compared to pure lipid vesicles. Both the enhanced $\nu_a(COO^-)$ mode and the lack of substantial changes in lipid melting indicate a Ca^{2+}-mediated charge-based interaction between SP-A and the DPPC headgroup.

Monolayers. Several recent reports have found that interfacial recognition processes between lipid monolayers and soluble proteins depend on the phase state of the lipid (*51*, *54*−*56*). Investigations of the interaction of two phospholipase enzymes with lipid monolayers found that different lipid phase states were preferred by the adsorbed proteins. PM (polarization modulation)-IRRAS was used to determine that the extent of hydrolysis catalyzed by phospholipase D increased when the lipid was in the liquid-expanded state (*55*), and fluorescence microscopy and GIXD were used to examine interfacial recognition as phospholipase A_2 adsorbed to lipid monolayers (*54*). In the second study, the enzyme was found to preferentially accumulate at LE/LC boundaries and to substantially reduce the tilt angle of lipid acyl chains in a manner similar to the current SP-A studies.

Early bulk-phase studies first established SP-A's preference for gel-state lipids (*15*, *21*). More recent fluorescence microscopy studies have shown a strong surface pressure/lipid phase dependence for the adsorption of SP-A to DPPC monolayers (*14*, *25*). At $\pi < 4$ mN/m (LE phase), labeled SP-A could not be visualized; however, once LC domains of DPPC appeared ($\pi \approx 10$ mN/m), the protein was found to accumulate at the LE/LC boundary. At $\pi \geq 30$ mN/m, SP-A was predominantly excluded from the lipid monolayer (*14*). Our observation of the enhanced amide I band intensity along with a slightly larger increase in surface pressure upon SP-A adsorption to a DPPC monolayer at $\pi_i = 10$ mN/m compared to 25 mN/m is also consistent with this lipid-phase dependence. A similar surface pressure/lipid-phase-dependent alteration is observed for DPPC acyl chain orientation in the current IRRAS experiments. A significant decrease in the average tilt angle from 35° to 28° was observed upon SP-A adsorption at $\pi_i = 10$ mN/m, but not at $\pi_i = 25$ or 40 mN/m. The SP-A-induced increase in lipid packing efficiency as tilt angle decreases over a certain pressure range may be important in the execution of specific SP-A functions at the air/alveolar interface. For example, SP-A has been shown to augment the transfer of phospholipids to the air/water interface in cooperation with the hydrophobic surfactant protein SP-B (*23*).

The amide I band shape was found to be quite similar under the different monolayer conditions studied (in the presence/absence of Ca^{2+} or DPPC). This similarity may be attributed to the presence of NaCl in the subphase as physiological concentrations of NaCl are known to induce SP-A self-association of octadecamers in solution (*12*).

Further aggregation, such as that induced by Ca^{2+} and/or the presence of a DPPC monolayer, without secondary structure alterations would not cause changes in the IRRAS amide I band shape. The increase in amide I band intensity, however, observed in the presence of Ca^{2+}, is most likely due to an enhancement in the amount of SP-A near the air/water interface (Figure 7). TEM observations of an SP-A collagen-deletion mutant show an increased association between the protein and lipid monolayer in the presence of Ca^{2+} (*16*), consistent with the enhanced IRRAS amide I band intensity.

The similarity in amide I band shape and position observed when comparing SP-A's bulk-phase IR and IRRAS spectra is notable (see Figure 7 inset). Whereas proteins and peptides have often been observed to change conformation or denature at the air/water interface compared to bulk-phase solution (*47*−*50*), the secondary structures of lung surfactant proteins SP-B, SP-C, and now SP-A have all displayed a resistance to conformational change in monolayer environments (*28*, *57*).

An important general result from the current studies is the persistence of SP-A's native secondary structure in diverse environments (monolayers, bulk phases). This would seem to be essential for the protein to efficiently execute a variety of functions in environments as varied as the alveolar hypophase and the air/alveolar interface. Future investigations of the structure of SP-A mutants under different conditions may reveal the essential structural constituents necessary for the protein's remarkable stability.

REFERENCES

1. Goerke, J., and Clements, J. A. (1986) in *Handbook of Physiology: The Respiratory System III* (Mackelm, P. T., and Mead, J., Eds.) pp 247−261, American Physiology Society, Washington, DC.
2. Veldhuizen, E. J. A., and Haagsman, H. P. (2000) *Biochim. Biophys. Acta 1467*, 255−270.
3. Goerke, J. (1998) *Biochim. Biophys. Acta 1408*, 79−89.
4. Creuwels, L., van Golde, L. M. G., and Haagsman, H. P. (1997) *Lung 175*, 1−39.
5. Johansson, J., and Curstedt, T. (1997) *Eur. J. Biochem. 244*, 675−693.
6. McCormack, F. X. (1998) *Biochim. Biophys. Acta 1408*, 109−131.
7. Eggleton, P., and Reid, K. B. (1999) *Curr. Opin. Immunol. 11*, 28−33.
8. King, R. J., Simon, D., and Horowitz, P. M. (1989) *Biochim. Biophys. Acta 1001*, 294−301.
9. McCormack, F. X., Damodarasamy, M., and Elhalwagi, B. M. (1999) *J. Biol. Chem. 274*, 3173−3181.
10. Voss, T., Eistetter, H., Schäfer, K. P., and Engel, J. (1988) *J. Mol. Biol. 201*, 219−227.
11. Haagsman, H. P., White, R. T., Schilling, J., Lau, K., Benson, B. J., Golden, J., Hawgood, S., and Clements, J. A. (1989) *Am. J. Physiol. 257*, L421−L429.
12. Haagsman, H. P., Sargeant, T., Hauschka, P. V., Benson, B. J., and Hawgood, S. (1990) *Biochemistry 29*, 8894−4900.
13. Ruano, M. L. F., Miguel, E., Perez-Gil, J., and Casals, C. (1996) *Biochem. J. 313*, 683−689.
14. Ruano, M. L. F., Nag, K., Worthman, L. A., Casals, C., Perez-Gil, J., and Keough, K. M. W. (1998) *Biophys. J. 74*, 1101−1109.
15. King, R. J., Carmichael, M. C., and Horowitz, P. M. (1983) *J. Biol. Chem. 258*, 10672−10680.
16. Palaniyar, N., McCormack, F. X., Possmayer, F., and Harauz, G. (2000) *Biochemistry 39*, 6310−6316.
17. Palaniyar, N., Ridsdale, R. A., Holterman, C. E., Inchley, K., Possmayer, F., and Harauz, G. (1998) *J. Struct. Biol. 122*, 297−310.
18. Ross, G. F., Notter, R. H., Meuth, J., and Whitsett, J. A. (1986) *J. Biol. Chem. 261*, 14238−14291.
19. Walther, F. J., David-Cu, R., Leung, C., Bruni, R., Hernandez-Juviel, J., Gordon, L. M., and Waring, A. J. (1996) *Pediatr. Res. 39*, 938−946.
20. Kuroki, Y., and Akino, T. (1991) *J. Biol. Chem. 266*, 3068−3073.
21. Casals, C., Miguel, E., and Perez-Gil, J. (1993) *Biochem. J. 296*, 585−593.
22. Suzuki, Y., Fujita, Y., and Kogishi, K. (1989) *Am. Rev. Respir. Dis. 140*, 75−81.
23. Hawgood, S., Benson, B. J., Schilling, J., Damm, D., Clements, J. A., and White, R. T. (1987) *Proc. Natl. Acad. Sci. U.S.A. 84*, 66−70.
24. Cockshutt, A. M., Weitz, J., and Possmayer, F. (1990) *Biochemistry 29*, 8424−8429.
25. Taneva, S., and Keough, K. M. W. (2000) *Biochemistry 39*, 6083−6093.
26. Flach, C. R., Gericke, A., and Mendelsohn, R. (1997) *J. Phys. Chem. 101*, 58−65.
27. Flach, C. R., Xu, Z., Bi, X., Brauner, J. W., and Mendelsohn, R. (2001) *Appl. Spectrosc. 55*, 1060−1066.
28. Gericke, A., Flach, C. R., and Mendelsohn, R. (1997) *Biophys. J. 73*, 492−499.
29. Wu, F., Corsico, B., Flach, C. R., Cistola, D. P., Storch, J., and Mendelsohn, R. (2001) *Biochemistry 40*, 1976−1983.
30. Mendelsohn, R., Brauner, J. W., and Gericke, A. (1995) *Annu. Rev. Phys. Chem. 46*, 305−334.
31. Taneva, S., McEachren, T., Stewart, J., and Keough, K. M. W. (1995) *Biochemistry 34*, 10279−10289.
32. Haagsman, H. P., Hawgood, S., Sargeant, T., Buckley, D., Tyler, W. R., Drickamer, K., and Benson, B. J. (1987) *J. Biol. Chem. 262*, 13877−13880.
33. Laemmli, U. K. (1970) *Nature 227*, 680−685.
34. Nielson, D. W. (1983) *Pediatr. Res. 17*, 386A.
35. Cameron, D. G., Kauppinen, J. K., Moffatt, D. J., and Mantsch, H. H. (1982) *Appl. Spectrosc. 36*, 245−250.
36. Noda, I. (1990) *Appl. Spectrosc. 44*, 550−561.
37. Gericke, A., Gadaleta, S. J., Brauner, J. W., and Mendelsohn, R. (1996) *Biospectroscopy 2*, 341−351.
38. Kuzmin, V. L., and Michailov, A. V. (1981) *Opt. Spectrosc. 51*, 383−385.
39. Kuzmin, V. L., Romanov, V. P., and Michailov, A. V. (1992) *Opt. Spectrosc. 73*, 3−47.
40. Bertie, J. E., Ahmed, M. K., and Eysel, H. H. (1989) *J. Phys. Chem. 93*, 2210−2218.
41. Fraser, R. D. B., and MacRae, T. P. (1973) *Conformation in Fibrous Proteins and Related Synthetic Polypeptides*, Academic Press, New York.
42. Haris, P. I., and Chapman, D. (1996) in *Infrared Spectroscopy of Biomolecules* (Mantsch, H. H., and Chapman, D., Eds.) pp 239−278, Wiley-Liss, Inc., New York.
43. Lazarev, Y. A., Grishkovsky, B. A., and Khromova, T. B. (1985) *Biopolymers 24*, 1449−1478.
44. Venyaminov, S. Y., and Kalnin, N. N. (1990) *Biopolymers 30*, 1243−1257.
45. Barth, A. (2000) *Prog. Biophys. Mol. Biol. 74*, 141−173.
46. McCormack, F. X., Stewart, J., Voelker, D. R., and Damodarasamy, M. (1997) *Biochemistry 36*, 13963−13971.
47. MacRitchie, F. (1989) *Chemistry at Interfaces*, Academic Press, Inc., San Diego, CA.
48. Chen, H., Hsu, S. L., and Tirrell, D. A. (1997) *Langmuir 13*, 4775−4778.
49. Dieudonné, D., Gericke, A., Flach, C. R., Jiang, X., Farid, R. S., and Mendelsohn, R. (1998) *J. Am. Chem. Soc. 120*, 792−799.
50. Wu, F., Gericke, A., Flach, C. R., Mealy, T. R., Seaton, B. A., and Mendelsohn, R. (1998) *Biophys. J. 74*, 3273−3281.
51. Zhao, J., Vollhardt, D., Brezesinski, G., Siegel, S., Wu, J., Li, J. B., and Miller, R. (2000) *Colloids Surf. 171*, 175−184.

52. Ruano, M. L. F., Garcia-Verdugo, I., Miguel, E., Perez-Gil, J., and Casals, C. (2000) *Biochemistry 39*, 6529−6537.
53. Yu, S.-H., McCormack, F. X., Voelker, D. R., and Possmayer, F. (1999) *J. Lipid Res. 40*, 920−929.
54. Dahmen-Levison, U., Brezesinski, G., and Mohwald, H. (1998) *Thin Solid Films 327−329*, 616−620.
55. Estrela-Lopis, I., Brezesinski, G., and Mohwald, H. (2001) *Biophys. J. 80*, 749−754.
56. Maierhofer, A. P., Bucknall, D. G., and Bayerl, T. M. (2000) *Biophys. J. 79*, 1428−1437.
57. Pastrana-Rios, B., Taneva, S., Keough, K. M. W., Mautone, A. J., and Mendelsohn, R. (1995) *Biophys. J. 69*, 2531−2540.

BI011188H